

ANALYSIS OF FISSION PRODUCT RELEASE BEHAVIOR
DURING THE TMI-2 ACCIDENT^a

D. A. Petti, J. P. Adams, J. L. Anderson, and R. R. Hobbins
Idaho National Engineering Laboratory
EG&G Idaho, Inc.
P.O. Box 1625
Idaho Falls, Idaho 83415

ABSTRACT

An analysis of fission product release during the Three Mile Island Unit 2 (TMI-2) accident has been initiated to provide an understanding of fission product behavior that is consistent with both the best estimate accident scenario and fission product results from the ongoing sample acquisition and examination efforts. "First principles" fission product release models are used to describe release from intact, disrupted, and molten fuel. Conclusions relating to fission product release, transport, and chemical form are drawn.

1. INTRODUCTION

The March 1979 accident at Three Mile Island Unit 2 (TMI-2), the most severe core damage accident that has occurred in a U.S. commercial light water reactor, provides a unique opportunity to obtain data about fission product behavior under real accident conditions. A significant fraction of the more volatile fission products was released from the fuel; however, these fission products were confined in the reactor coolant and other plant systems and the containment without significant release to the environment. Examining the dominant physical and chemical processes that affected fission product release behavior during the accident may improve the current understanding of such phenomena as fission product release, transport, and chemical form, an understanding that is currently based largely on separate effects and scaled integral test data. Thus, the accident provides the only full-scale data base with which to study these phenomena. The DOE has sponsored a major program at the INEL to maximize the quantity and quality of this data base. This program is the TMI-2 Accident Evaluation Program and its objective and plan are documented in Reference 1.

The purpose of the work reported here is to analyze fission product release from the core during the accident using "first principles" fission product release models. The results from this study will be used to improve our understanding of the accident scenario and to provide additional insight into the accident. The fission product release and retention estimates developed

a. Work supported by the U.S. Department of Energy Assistant Secretary for Nuclear Energy, Office of Light Water Reactor Safety and Technology, under DOE Contract No. DE-AC07-76ID01570.

in this study will be compared, to the extent possible, with retention data from samples that have and will be obtained from TMI.

Brief reviews of the accident scenario and the fission product retention data from TMI-2 are presented in Section 2. Sections 3 through 6 describe the proposed "first principles" analyses that will be used to describe fission product release during the TMI-2 accident. A summary and conclusions from this work are provided in Section 7.

2. REVIEW OF THE TMI-2 ACCIDENT SCENARIO AND FISSION PRODUCT RETENTION DATA

2.1 Accident Scenario

The fission product analysis has been divided into four parts to correspond to the four thermal/hydraulic phases of the accident. Each phase represents a different set of core thermal/hydraulic and fuel conditions. This section will briefly review the five phases of the TMI-2 accident. Additional information about the accident scenario is provided in Reference 2.

Phase 1 is defined as the time from the turbine trip (time zero) until the A-loop reactor coolant pumps (RCPs) were turned off at 100 min. (The B-loop RCPs were turned off earlier at 73 min.) This phase is characterized as a small-break LOCA accompanied by a slow depressurization of the reactor coolant system without uncover or heatup of the core. Hence, no fission product release occurred.

The thermal and hydraulic conditions during Phase 2 (between cessation of forced convection at 100 min and the B-pump transient at 174 min) were characteristic of a slow core boiloff and heatup that started between 114 and 120 min, and continued throughout this phase. Containment radiation monitor signals indicated that some fuel rods had burst between 137 and 142 min. High output currents were observed from the SPNDs in the central upper region. At approximately 150 min, it is believed that rapid oxidation had begun causing cladding temperatures to exceed 1850 K. This exothermic oxidation drove temperatures above clad melting and some fuel dissolution began. Downward relocation of this liquefied material would be expected to occur, resulting in a small blockage of material near the core center. Core heatup analysis indicates that peak core temperatures exceeded 2400 K by 174 min. The upper portions of the core contained partially oxidized rods and high temperature remnants consisting of UO_2 pellets and ZrO_2 cladding. In the central region of the core, a partially molten noncoolable U-Zr-O mixture rested upon a hard pan of ZrO_2/UO_2 ceramic which had solidified between the existing fuel rods.

Phase 3 is defined as the time period between 174 and 224 min. For the purposes of the fission product analysis, this phase is separated into two phases termed Phases 3a and 3b. Phase 3a is termed the "B-pump" transient because the 2B RCP was operated for a short time (several tens of minutes) and introduced about 28 m^3 of water in an effort to cool the core. The

pump transient caused the highly brittle oxidized cladding to fracture, forming a rubble bed of fuel pieces and cladding shards which rested on the molten U-Zr-O mixture.

During Phase 3b between 180 and 224 min, the molten U-Zr-O material and part of the debris bed continued to heat to produce a large molten mass surrounded by a crust. This occurred despite the fact that the liquid level was estimated to be near the top of the core. On top of the crust is a debris bed and a void region formed when the embrittled fuel rods collapsed during Phase 3a. A simplified one-dimensional heatup analysis of the molten mass and the surrounding upper and lower crusts indicates that despite the limited cooling at the periphery the molten material continued to heat up from decay heat due to the high thermal resistance of the oxide and the large thermal capacitance of such a large consolidated mass.

Selected data from the accident substantiate that during the last phase, Phase 4, which lasted from 224 to 230 min, a major relocation of core material occurred. Visual inspection data and crust failure analysis indicate that the crust surrounding the molten pool failed near the top at the southeast core periphery. The molten material then drained through the lower support assembly and into the lower plenum. It is estimated that between 10 and 20 tons of core material relocated to the lower plenum at this time.

As is noted in Reference 2, the accident scenario represents a best-estimate interpretation of the TMI-2 data to date. Work is continuing to define more details, especially from the later phases of the accident. Hence, the understanding of the accident scenario might change.

2.2 Fission Product Retention

The fission product inventory at the time of the accident is needed for the release calculations presented here. Table 1 lists the inventories for various fission products based on a detailed nodal ORIGEN2 inventory calculation.[3]

Small samples from the upper debris bed and the lower plenum have been analyzed for their fission product content.[4] The average fission product retentions for ^{106}Ru , ^{125}Sb , ^{129}I , ^{137}Cs , ^{90}Sr , ^{154}Eu , and ^{144}Ce are presented in Table 2 along with the range found in the various debris samples. One objective of this work is to explain the results in Table 2, especially the high retention of the cesium in the lower plenum samples, the high retention of iodine in the upper debris samples, and the low retention of ruthenium in the lower plenum samples.

3. FISSION PRODUCT RELEASE DURING PHASE 2

During the initial core heatup and degradation, three mechanisms are thought to contribute to fission product release: gap release, diffusional release, and release from liquefied fuel. Because the burnup of fuel in TMI-2 was

TABLE 1. TOTAL CORE ELEMENTAL FISSION PRODUCT INVENTORIES

<u>Element</u>	<u>Inventory^a (moles)</u>
Kr	42.6
Sr	129.6
Ru	176.1
Sb	2.2
Te	29.2
I	17.3
Xe	314.4
Cs	161.7
Ce	209.9
Eu	3.5

a. Three hours after scram (from Reference 3).

TABLE 2. AVERAGE FISSION PRODUCT RETENTION

<u>Radionuclide</u>	<u>Percent of Inventory Retained^a</u>			
	<u>Lower Plenum</u>		<u>Upper Plenum</u>	
	<u>Average</u>	<u>Range</u>	<u>Average</u>	<u>Range</u>
I-129	3	3- 24	22	10- 38
Cs-137	14	0- 38	21	6- 32
Ru-106	7	0- 19	55	35- 86
Sb-125	3	0- 17	23	18- 38
Sr-90	114	73-190	93	79-102
Eu-154	86	69-105	90	60-108
Ce-144	110	90-164	114	90-130

a. Compared with core average ORIGEN-2 analysis ($\mu\text{Ci/gU}$).

quite low (<4000 MWd/MTU), very little fission product inventory is expected to have been in the gap. As a result, gap release will not be examined here. This section will discuss models that have been used to describe diffusional release and release from liquefied fuel.

3.1 Booth Diffusion Model

Many out-of-pile postirradiation experiments [5-8] indicate that for temperatures between 1000 and 2180 K prior to fuel dissolution, fission product behavior is dominated by diffusional release of volatile fission products (Xe, Kr, Cs, I, Te) from ruptured fuel rods. Very little release of the medium and low volatile fission products is expected for these temperatures. Many investigators have used the Booth diffusion model [9] has been used successfully to describe the results of fission product release experiments conducted in this temperature range. The Booth diffusion model is based on the solution to the diffusion equation from a sphere of radius a . The fractional release of a fission product is given by

$$FR = 6(Dt/\pi a^2)^{1/2} - 3Dt/a^2 \quad (1)$$

where

- D = diffusion coefficient of the fission product (cm^2/s)
- a = "equivalent radius" of the sphere (cm)
- t = time (s).

The diffusion coefficient is usually given by an Arrhenius function of the form

$$D = D_0 \exp(-Q/RT) \quad (2)$$

where

- D_0 = pre-exponential factor (cm^2/s)
- Q = fission product activation energy (kcal/mole)
- R = universal gas constant (kcal/mole K)
- T = fuel temperature (K)

and the equivalent radius is derived from the total surface area available for diffusion and the volume of the specimen. In general, this latter parameter is difficult to obtain for specimens that are poly-crystalline. As a result, many researchers correlate their results to an effective diffusion coefficient D' where $D' = D/a^2$.

The Booth model given by Equation (1) is applicable for the case of a constant temperature anneal and releases less than 30%. The temperatures in TMI-2 were not constant during the initial core heatup; hence the diffusion coefficients [Equation (2)] changed with time. As a result, the Booth diffusion model has been modified to account for the transient temperature

response of the core. For a transient temperature, an infinite series form of the solution is used. The fractional retention is given by

$$\text{Fractional retention} = \frac{6}{\pi^2} \sum_{n=1}^{\infty} \frac{1}{n^2} \exp(-n^2 \pi^2 \tau) \quad (4)$$

where

$$\tau = \frac{1}{a^2} \int_0^t D[T(t')] dt' .$$

The fractional release rate, dFR/dt , is given by

$$\frac{dFR}{dt} = \frac{6D(t)}{a^2} \sum_{n=1}^{\infty} \exp(-n^2 \pi^2 \tau) . \quad (5)$$

Thus, for a given node in the TMI-2 core, the release fraction and fractional release rate for the volatile fission products can be calculated once the temperature history has been established and reasonable values of D and a have been chosen.

The core temperature history that was used in this calculation was determined using the SCDAP/RELAP5 computer code.[10] The core was modeled using three representative radial fuel regions, corresponding to the center, middle, and peripheral regions of the core. Six axial nodes were used to model each fuel region resulting in a total of 18 nodes for the entire core. Figure 1 is a schematic representation of the reactor core and vessel nodalization used for this calculation. Cladding temperatures were calculated from accident initiation to the end of Phase 3a, or 180 min. Figure 2 presents the calculated cladding temperatures from 100 to 180 min for the center, middle, and peripheral assemblies in the core. Booth diffusion is a valid representation of fission product behavior only as long as the fuel geometry is preserved. Therefore, the calculation of fission product release was carried out only up to a temperature of 2180 K (temperature at which dissolution of UO_2 by molten zircaloy begins) in the base case calculation.

The expression for the diffusion coefficient, D , was extracted from an extensive study by Lawrence.[11] This study investigated the influence of several environmental conditions on the diffusional release of fission products, including postirradiation anneal versus in-pile testing, stoichiometry, burn-up, fuel density, power rating, and surface vaporization and sublimation. The data base used in determining the best-estimate diffusion coefficient for Xe included data from postirradiation annealing experiments with fuel densities ranging from 58 to 99% of theoretical,

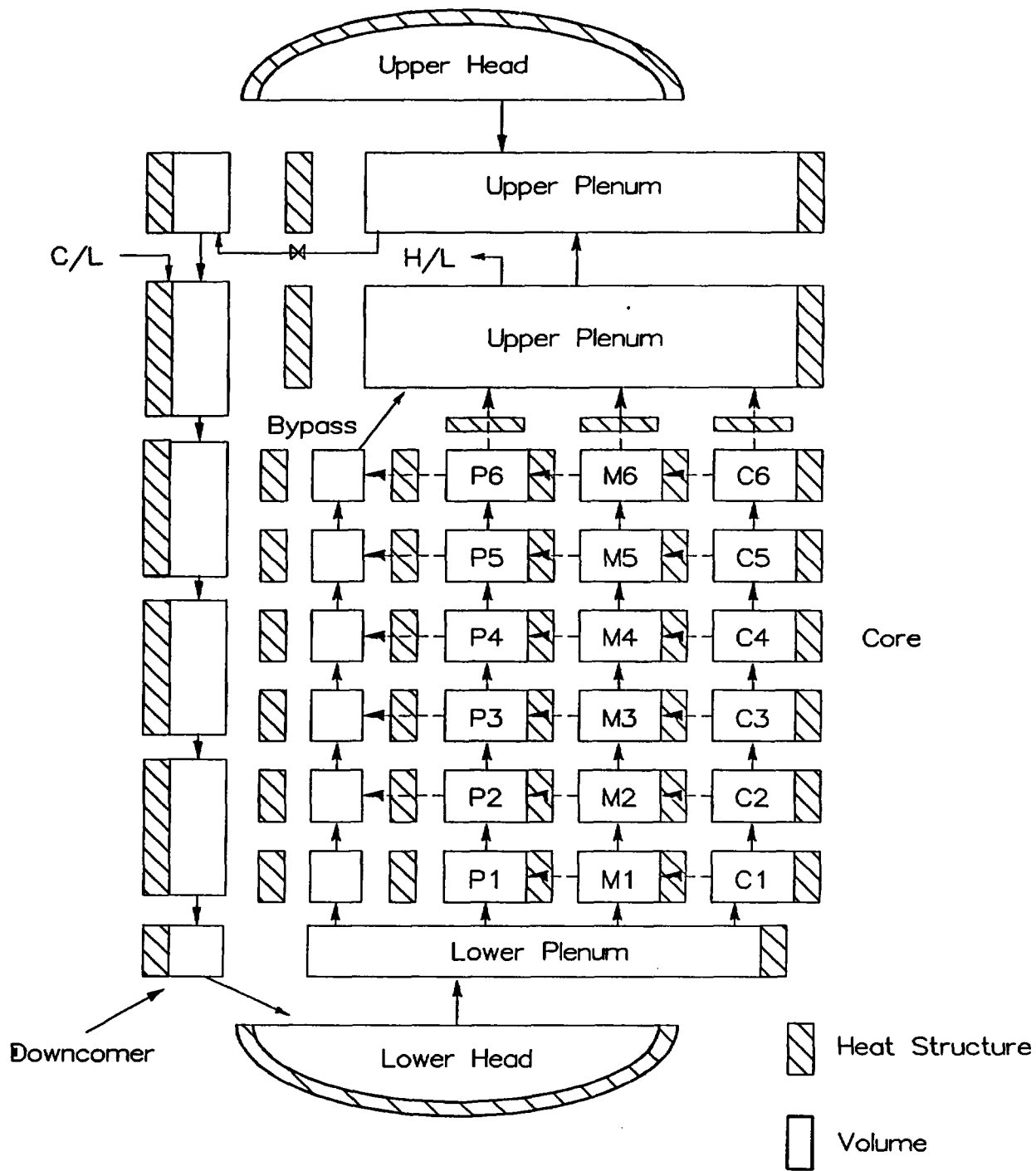


Figure 1. SCDAP/RELAP5 nodalization of the TMI-2 reactor vessel and internals.

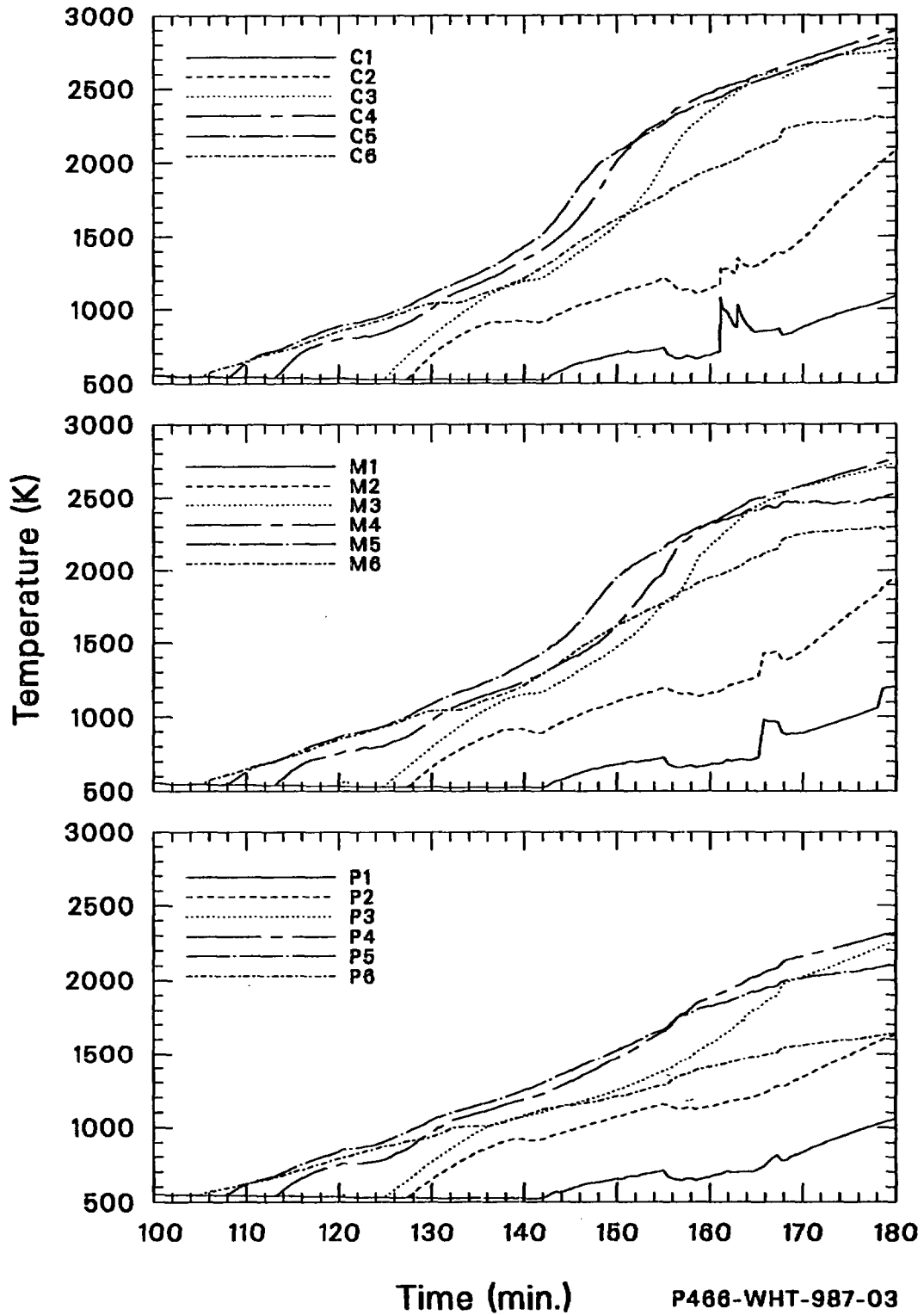


Figure 2. SCDAP/RELAP5 temperature calculations for the TMI-2 accident between 100 and 180 min.

stoichiometry ranging from 1.9 to 2.22, temperatures ranging from 870 to 2470 K, and burnups up to 800 MWD/MTU. The resultant diffusion coefficient for Xe was determined to be

$$D = 7.6 \text{ E-06 } \exp(-7.0 \text{ E+04}/RT) \text{ cm}^2/\text{s} \quad (6)$$

The sphere radius, a , used in this study was derived from a correlation developed by Belle, [12] illustrated in Figure 3. The least squares fit to the data by Belle, also shown in this figure is [13]

$$a = 3R \cdot 10^{[20.61 - R(67.9 - 46R)]} \quad (7)$$

where R is the ratio of the fuel density to theoretical density. The density of the fuel used in the TMI-2 core was 92.5% [14] which corresponds to an effective sphere radius of 4.0 E-03 cm . Equation (6) was divided by the square of this effective radius to obtain the fractional release rate versus temperature. This result is plotted in Figure 4.

These three input parameters (calculated core temperatures, diffusion coefficient, and effective sphere radius) were used to estimate Xe release for temperatures up to 2180 K in the base case calculation. In addition, a series of sensitivity studies were made wherein the core temperatures, diffusion coefficient, effective sphere radius, and maximum temperature were varied to bound the expected fission product release. The core temperatures were varied by $\pm 100 \text{ K}$ because of uncertainties in the SCDAP/RELAP5 temperature calculation. A second correlation for the diffusion coefficient, developed by Prussin et al., [8] was used to investigate the sensitivity of the results to this parameter. This correlation is also plotted in Figure 4. The effective sphere radius was varied from 2.0 E-03 (corresponding to the low range of the fuel pellet density) to 2.0 E-02 cm (corresponding to the maximum expected radius in Reference 8). Finally, the maximum temperature up to which the Booth analysis was considered valid was varied between 1700 and 2800 K, the lower temperature corresponding to liquefaction of the steel components in the core and the upper temperature corresponding to the monotectic temperature at which there is an enhanced solubility of UO_2 in molten zircaloy.

Xenon release results for the base case and sensitivity calculations are listed in Table 3. Xenon release was found to be most sensitive to the maximum temperature used in the calculation. As noted, the base case calculation, as well as nearly all of the sensitivity calculations, indicate only minimal (<2%) release of fission product Xe due to diffusion during Phase 2. This low total release is the result of the generally small calculated release rates (on the order of $5 \text{ E-03 } \%/s$). The exception is for the upper bound calculation, designated number 9 in Table 3. For this calculation, all of the parameters were set to result in the maximum expected release, including the largest diffusion coefficient, highest maximum temperature, and highest cladding temperatures. The resulting core-average release was 27%. Thus, the core-average release of Xe (and by implication, Kr, I, and Cs) is calculated to be between 0 and 27%.

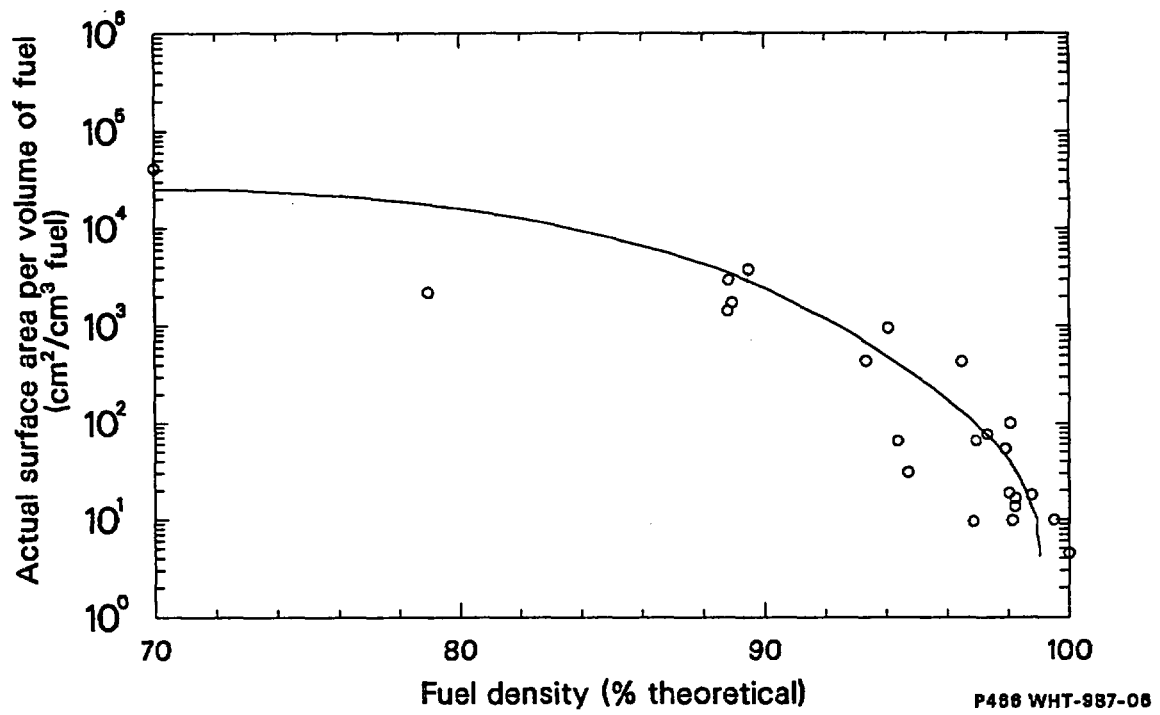


Figure 3. Effective surface-to-volume ratio as a function of theoretical density.

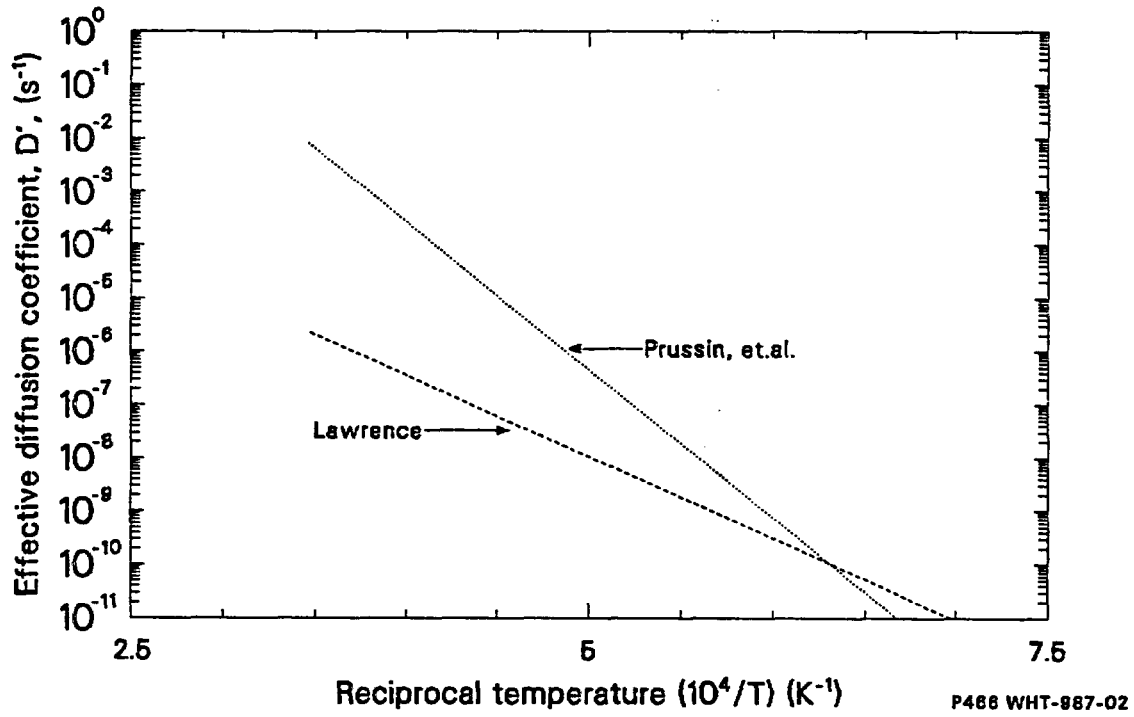


Figure 4. Diffusion coefficient correlations used in the Booth diffusional release calculation.

TABLE 3. CALCULATED DIFFUSIONAL RELEASE FROM TMI CORE DURING PHASE 2

<u>Number</u>	<u>Calculation</u>	<u>Percent Release</u>
1	Base case	0.02
2	$T = T_{SCDAP} + 100$	0.05
3	$T = T_{SCDAP} - 100$	0.01
4	$a = 0.02$ cm	0.002
5	$a = 0.002$ cm	0.09
6	$T_{max} = 2800$ K	0.68
7	$T_{max} = 1700$ K	0.002
8	Prussin results	1.77
9	All parameters at maximum values	27.0
10	All parameters at minimum values	0.000

Though the core-average release was in the range between 0 and 27%, individual nodes were calculated to have released up to 60% of their inventory, depending on their location in the core and the temperature history. The range of core nodal release fractions is indicated in Figure 5 which shows the release fraction histories for the nodes experiencing the maximum and minimum releases as calculated for the base case and maximum release calculations, respectively. Also included is a node which experienced a release near the average for each case. As shown in the figures, the minimum nodal release was approximately 0 for both calculations while the maximum nodal release was approximately 60%.

The specific calculation, described above, was for the release of fission product Xe from the TMI-2 core. It has been assumed in this analysis that other gaseous and high volatile fission products (Kr, I, Cs, and Te) diffused at approximately the same rate. While it is obvious that there are differences in the diffusion of these different fission products, these differences are expected to be smaller than the uncertainties in the other parameters governing diffusion (e.g., calculated versus actual core temperatures, fuel stoichiometry, etc.). The effect of these differences on the release fractions is included within the sensitivity calculations already discussed.

A direct comparison of the calculated release fractions with measured data from the core cannot be made, primarily because of the difficulty involved in identifying the conditions experienced by individual samples extracted from the core and the uncertainty in identifying the original enrichment and burnup (both of which affect the initial fission product inventory) in the sample. Additionally, there are no samples available that experienced only the first two phases of the accident; therefore the measured fission product release fractions are a result of fission product release during the entire accident. Within these uncertainties, however, some general comparisons between measured and calculated fission product release can be made. Volatile fission product release measured in samples extracted from the upper

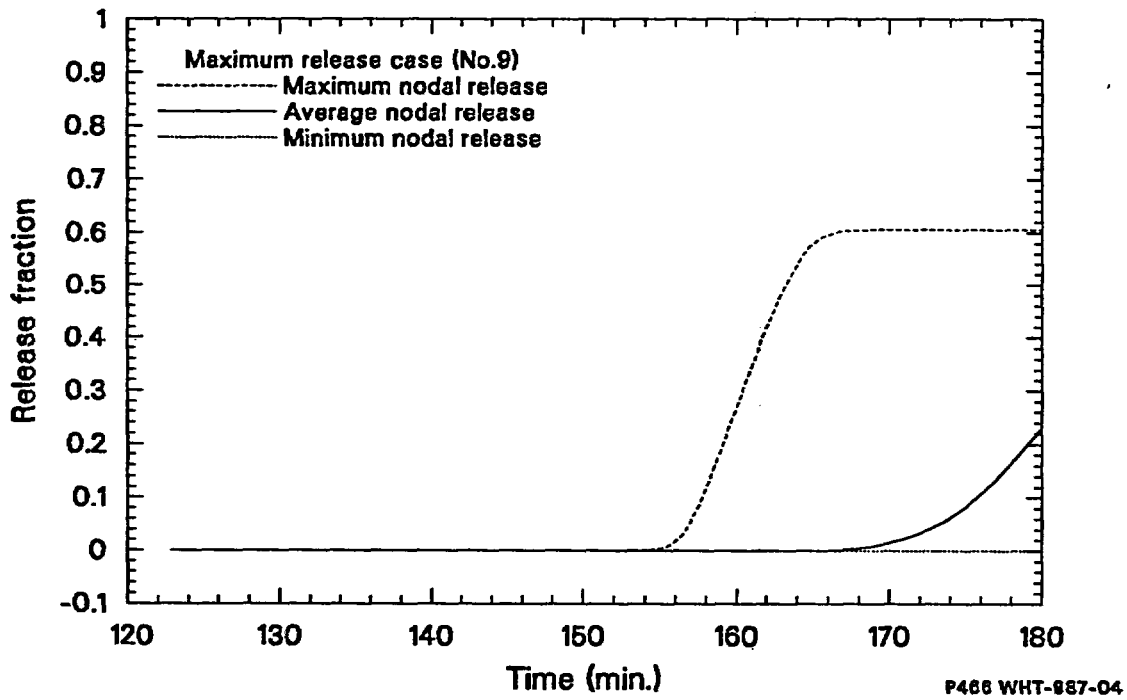
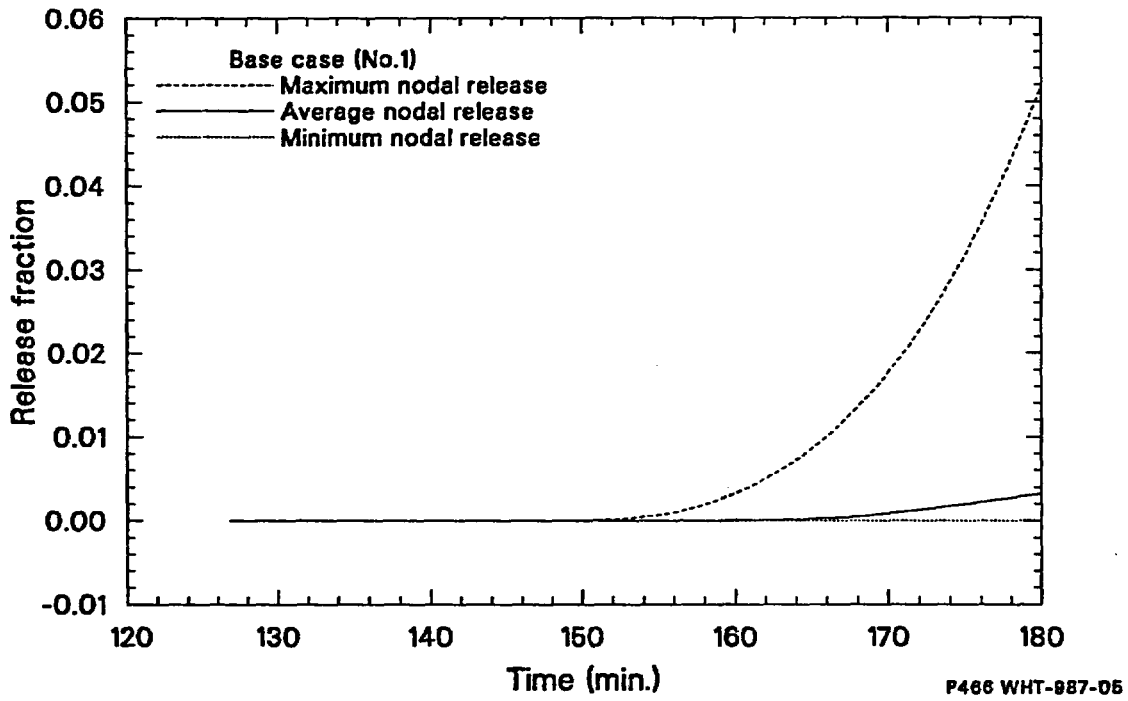


Figure 5. Nodal fractional release histories from the Booth diffusional release calculations.

debris bed is judged to have occurred primarily during Phases 2 and 3a since during Phases 3b and 4 this debris was covered with water and was in the process of being quenched. No data on noble gas release from these samples are yet available (but will become available in the future). Release of I and Cs from these samples ranges from 69 to 87% for I and from 60 to 92% for Cs. The calculated Phase 2 nodal releases for both of these species range from 0 to 60%, depending on the temperature and diffusivity parameters used in the calculation for the particular mode. Significant additional release is expected to have occurred during Phase 3a, as discussed in Section 4. Thus, these volatile fission product release calculations are generally consistent with the data obtained from the upper debris samples.

In general, Te release from the fuel pellets is roughly similar to the Xe diffusional results. However, separate effects test data indicate that Te tends to become bound to unoxidized Zr in the cladding. When the zircaloy oxidizes, the Te is released. It is recommended in Reference 15 that when the local Zr oxidation is less than 70%, the calculated Te release should be reduced by a factor of 40. It is indicated in Reference 16 that the global Zr oxidation was of the order of 50% (based on an analysis of the hydrogen that was evolved from the core). However, since approximately 40% of the core was largely undamaged (i.e., remained predominantly in an unoxidized rod-like geometry), the hydrogen generation estimate indicates that the damaged portion of the core could have been heavily (~80%) oxidized. Therefore, it is expected that in the undamaged core regions where the local oxidation is less than the 70% threshold, any Te released from the fuel would be sequestered by the cladding. However, for the heavily damaged areas of the core, significant Zr oxidation probably occurred, suggesting that the Te release from these regions could be large.

3.2 Other Factors Affecting Fission Product Release During Heatup

There are factors other than simple diffusion that affect fission product release from UO_2 during heatup of solid fuel. Two of the more important are fuel oxidation and fuel burnup. Fission product gases migrate to fuel grain boundaries during irradiation under normal operating conditions and collect in bubbles in the boundaries. Above burnups of ~5000 MWd/MTU, depending on the fuel temperature, the density of gas bubbles in the boundaries becomes great enough that the bubbles tend to interconnect to form a continuous tunnel network of voids in the grain boundaries that reaches to the pellet surface. This tunnel network provides a path of rapid escape for fission gases and vapors that reach it from the grain interiors. Because the average burnup in the TMI-2 core was <4000 MWd/MTU, this tunnel network would not be expected to be well developed prior to the accident. The microstructures of fuel in regions of the TMI-2 core not exposed to high temperatures in the accident confirm this expectation (Figure 6).

Oxidation of the fuel by steam enhances atomic mobility in the UO_2 and thus the release rates of fission products. Enhancements in release due to fuel oxidation by factors of 2 to 4 have been reported.[17] One of the evidences of the effect of increased atomic mobility is accelerated grain growth. The process of grain boundary sweeping during grain growth can be an important

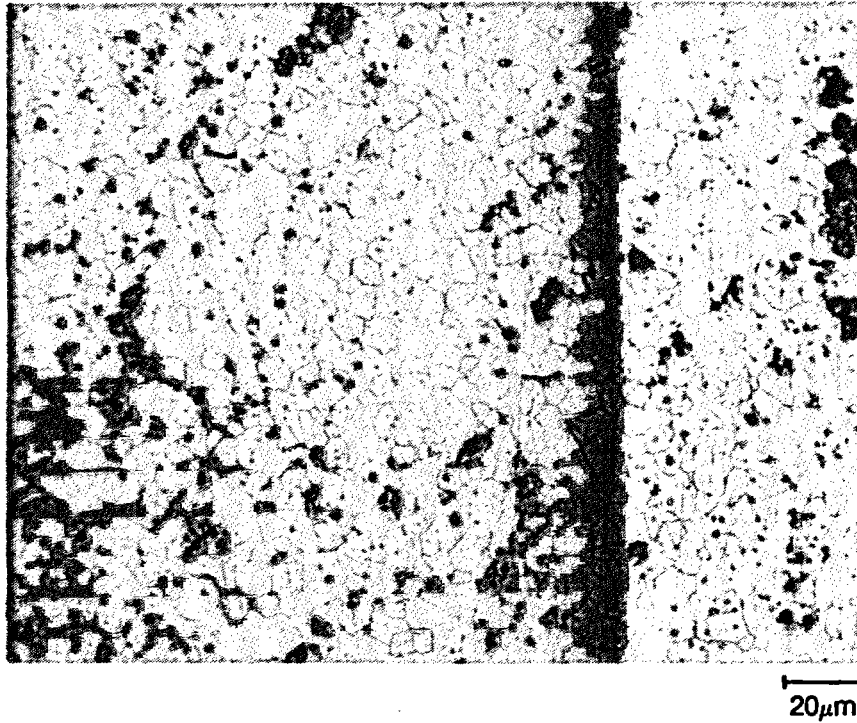


Figure 6. Optical photomicrograph of etched fuel below lower crust showing microstructure typical of low burnup fuel, i.e., little porosity redistribution. Sample from location D4, 1.05 m above bottom of core.

mechanism for accelerating the migration of fission products to grain boundaries during heatup. However, in low burnup fuel such as in TMI-2, the fission products accumulated at the grain boundaries during heatup are trapped until the boundaries are opened or otherwise changed by other phenomena. Therefore, although some evidence of at least localized fuel oxidation in TMI-2 exists,[18] the possible effects on fission product release are accommodated within the sensitivity study (discussed in Section 3.1) that varied the magnitude of the diffusion coefficient in the Booth model. Two additional phenomena that can affect the structure of the grain boundaries and the release of fission products trapped in them are fuel liquefaction and fuel cracking. Fuel liquefaction by interaction of UO_2 with molten zircaloy occurs upon heatup and is discussed in the following section, whereas fuel fracturing is of concern principally upon cooling and is discussed under Phase 3a.

3.3 Fission Product Release from Liquefied Fuel

Laboratory studies [19] of the liquefaction of UO_2 by molten zircaloy show that the process proceeds by the diffusion of oxygen from the UO_2 preferentially along grain boundaries into the zircaloy. The depletion of oxygen leads to reduction of the UO_2 to liquid uranium metal in the grain boundaries. The boundaries are weakened by this process and grains of UO_2 are separated from the surface of the fuel and are surrounded by molten zircaloy. The high surface area of the individual grains contributes to their rapid dissolution by the zircaloy. Once the UO_2 has been dissolved in the molten zircaloy, the release of fission gases and vapors is governed by the coalescence and rise of bubbles in the liquid to a free surface. This behavior is considered in the Phase 3b analysis.

It has been argued,[20] based on theories of atom and bubble mobilities, that the liquefaction of grain boundaries in low burnup fuel should cause an increase in the release rate of fission gases and volatile fission products (such as iodine and cesium), but should cause no significant change in release rates for high burnup fuel with interlinked porosity at grain boundaries. On-line measurements of fission product release rates from some in-pile bundle tests using trace-irradiated fuel have been interpreted in terms of enhanced release rates upon fuel liquefaction,[21,22] but these experiments are complex and not readily amenable to unambiguous interpretation. A reduction in fission product release rates has been calculated by Rest [23] for grain boundary liquefaction in out-of-pile release tests performed on high burnup fuel at Oak Ridge National Laboratory.[24] As will be discussed in Section 4.2, fuel fragments in the upper debris bed exhibit some degree of interlinked porosity in grain boundaries typical of higher burnup because of time at high temperature. Therefore, for the analysis of fission product release during the heatup phase in the TMI-2 accident, the effect of grain boundary liquefaction in TMI-2 fuel would not change fission product release rates significantly and that the effect is accommodated within the sensitivity study varied the magnitude of the diffusion coefficient in the Booth model. The effect of bulk dissolution of UO_2 by molten zircaloy is analyzed in Phase 3b where

bubble coalescence of fission product gases and vapors is considered and is found to have a pronounced effect on release from the liquid state.

4. FISSION PRODUCT RELEASE DURING PHASE 3A

Phase 3a is defined as the time period between 174 and 180 min when the B-loop pump was restarted and injected a large quantity of liquid into the vessel. No "first principles" models exist to characterize fission product behavior during the quenching of the fuel and formation of the debris bed which occurred in Phase 3a. Therefore, this section is limited to a discussion of in-pile experiments that were quenched from high temperature, and the results from metallurgical examination of the upper debris bed samples from the TMI-2 core.

4.1 Fission Product Release during Fuel Fracturing and Fragmentation

The Power Burst Facility Severe Fuel Damage Scoping Test (SFD-ST) [22] and the Loss-of-Fluid Test (LOFT) FP-2 experiment [25] are the only two severe fuel damage in-pile experiments in which the fuel bundle was cooled with a rapid reflood of water into the bundle. In SFD-ST greater than 90% of the fission product release occurred after initiation of reflood and preliminary information suggests that a similar release behavior occurred in the LOFT FP-2 experiment. The fuel burnup in these experiments was very low, less than 450 MWd/MTU. As was discussed above, one would expect fission products to migrate to grain boundaries in low burnup fuel during a high-temperature transient. The fuel will crack as it is subjected to thermal-mechanical stresses during cooling as a result of reflood. Transgranular and intergranular cracking have been observed in fuel cooled rapidly from high temperature. Intergranular cracking has been explained [26] based on quenching from above the equicohesive temperature (about 1900 K in UO₂) where the ultimate tensile strength sharply decreases due primarily to decreasing grain boundary strength and ductile failure along grain boundaries. (Note that in the SCDAP/RELAP5 calculation described in Section 3, nearly 90% of the upper half of the core reached temperatures in excess of 1900 K prior to the B-pump transient.) Some fracture along grain boundaries was observed in SFD-ST but this phenomenon was not widespread. Transgranular cracking can intersect accumulations of fission products trapped at grain boundaries and enhance release. This kind of cracking is prevalent in both SFD-ST and in the particles that make up the upper debris bed in TMI-2 (Figure 7).

4.2 Fuel Morphology of TMI-2 Upper Debris Bed Samples

Samples from the upper debris bed have been examined to characterize the fuel morphology that is important to fission product release before and during the pump transient. Specifically, the examination focused on characterizing grain boundary porosity and interconnection, the degree of fuel oxidation, fuel fracturing, and amount of grain growth. Figure 8 shows that the grain boundaries contain a great deal of porosity and that some interconnection to form tunnels along grain edges may have occurred.

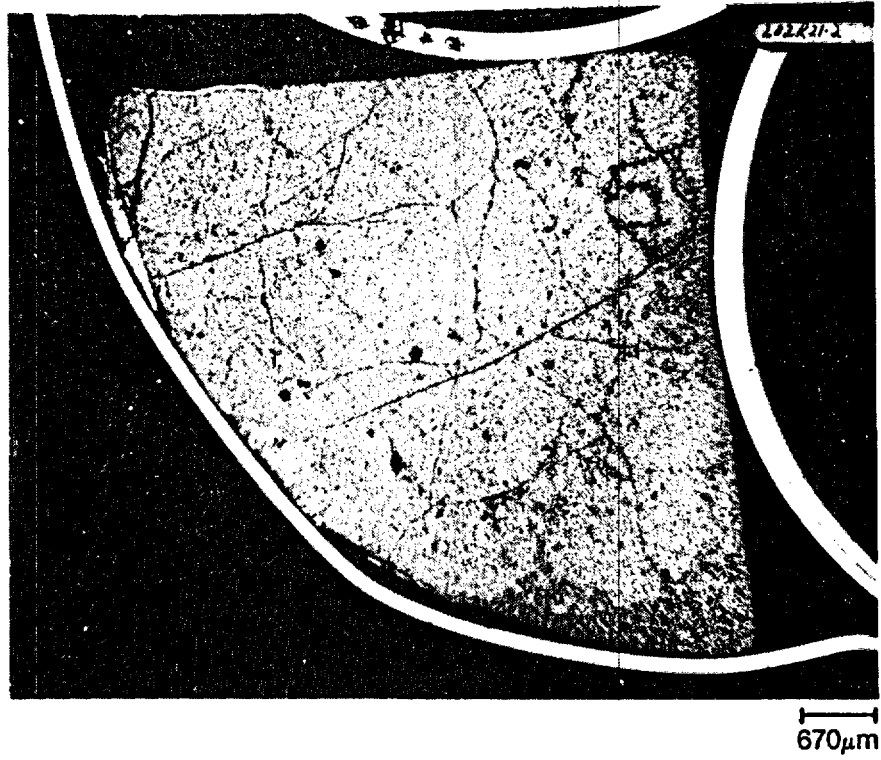


Figure 7. Macrocracking of fuel fragment in upper debris bed.

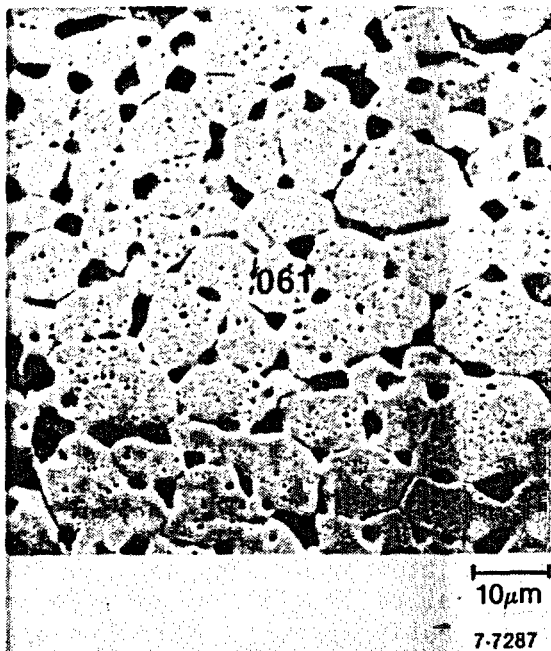


Figure 8. Scanning electron microscope image showing interlinked porosity at grain boundaries in fuel in the upper debris bed.

Based on the microstructure of fuel that was not overheated in the accident (Figure 6) and previous work,[20,24,27] it is expected that fission gas bubbles migrated to the grain boundaries primarily during the heatup in Phase 2 of the accident. To the extent that open pathways developed along grain boundary edges, fission gases and vapors could be released in this phase of the accident at a rate exceeding simple diffusion as calculated in Section 3.1. However, evidence of interaction of the fuel with molten zircaloy is widespread in the upper debris bed (Figure 9) and this interaction produces liquid uranium metal in the grain boundaries of the fuel,[19] tending to slow release along previously open pathways. Despite some Auger measurements indicating localized oxidation of the fuel, the absence of U_4O_9 in the microstructure suggests that fuel oxidation was not widespread. This observation is consistent with the observed lack of grain growth. There was a large amount of macrocracking evident in the fuel cross sections (Figure 7) and fuel pullout during preparation (Figure 10) indicating that grain boundary separation or intergranular cracking also occurred. The intersection of macrocracks with porosity trapped at grain boundaries has been used to explain fission gas release upon cooling from high temperature transients.[27] Additionally, grain boundary separation can contribute to fission product release upon reflood.

In summary, the microstructure of the fuel in the upper debris bed suggests that fission gas bubbles migrated to grain boundaries during the heatup period of the accident (Phase 2) and that some interlinkage accelerating fission product release from the fuel may have occurred. However, the reduction of UO_2 to uranium in grain boundaries by the interaction with zircaloy would be expected to occur in a similar temperature regime (2200 K) and, therefore, in a similar time frame, as the interlinkage of porosity along the boundaries. The net result is that fission product release during Phase 2 may not have been greatly affected by either grain boundary interlinkage or the initial stages of fuel liquefaction. The range of diffusivities employed in the Booth diffusion study of fission product release in Phase 2 is intended to encompass uncertainties in the phenomena discussed above. Although the release is not expected to be affected by the initial stages of fuel liquefaction, the release of fission gas bubbles from the liquid formed by bulk dissolution of UO_2 can be rapid as is discussed in the Phase 3b analysis. The macrocracks and fuel intergranular fracturing observed in the fuel in the upper debris bed suggest that considerable additional release of fission gases and volatile fission products could have taken place upon reflooding at the time of the B-loop pump transient.

5. FISSION PRODUCT RELEASE DURING PHASE 3B

Phase 3b is defined as the time period between 180 and 224 min when the consolidated mass of molten material was in an uncooled geometry surrounded by water. During this phase, this mass continued to heatup and form a large molten pool. This molten mass was surrounded by a crust which was covered with a debris bed. The core was covered with water as a result of the B-loop pump transient. Fission product release during this phase can come from three separate fuel regions: fuel still in a rod-like geometry, the debris bed, and the molten pool. Because the rods and debris bed were relatively

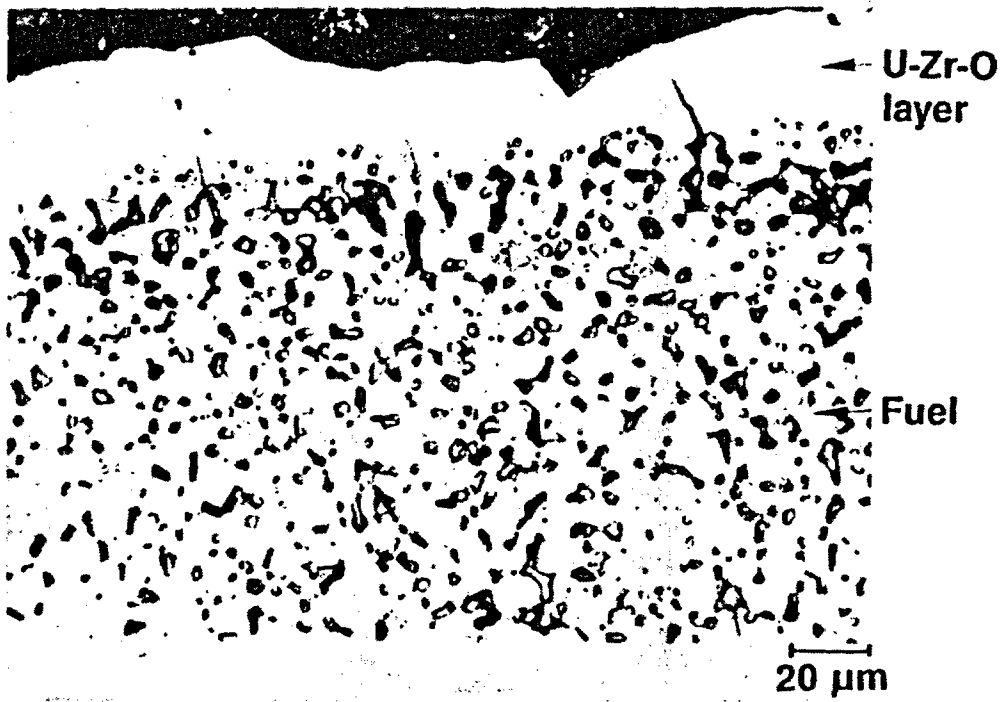


Figure 9. Optical photomicrograph showing interaction of molten zircaloy with fuel in upper debris bed.

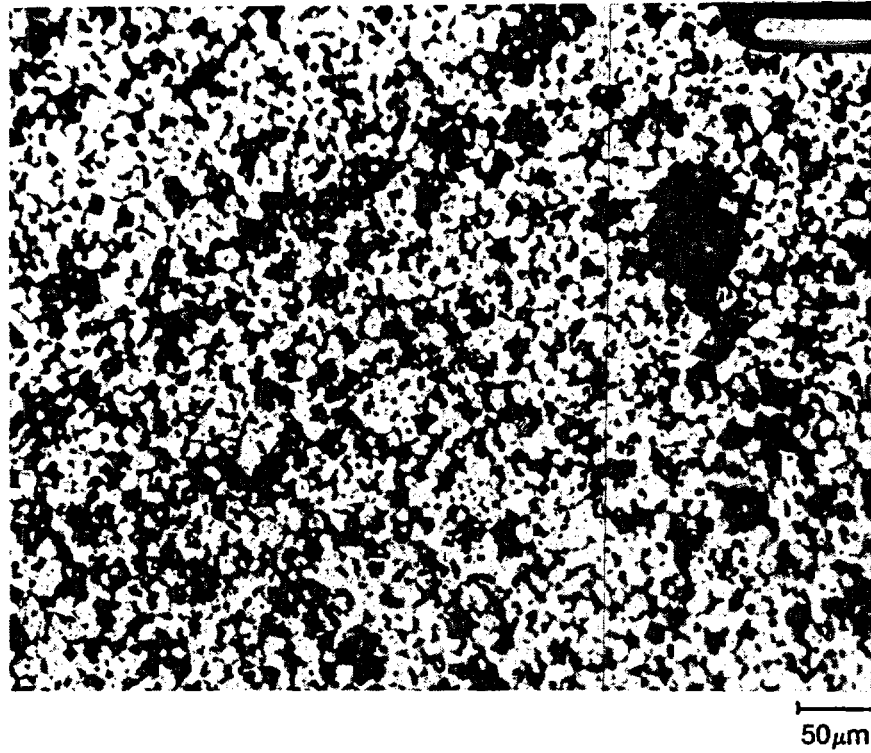


Figure 10. Optical photomicrograph showing fuel pullout due to intergranular fractures in fuel in the upper debris bed.

cool, very little fission product release is expected from these sources. As a result, only fission product release from the molten pool is considered here.

Details of the geometry of the molten pool used in all calculations in this section are given in Section 5.1. Different mechanisms are thought to govern the release of the high and low volatile fission products from the molten mass. Because the volatile fission products are gaseous at high temperature (>2800 K) their release is expected to be dominated by bubble dynamics in the molten pool. Section 5.2 examines bubble dynamics in a convective pool to determine the amount of gas that can be released from the melt. Medium and low volatile fission products (Sb, Sr, Eu, Ce) will tend to exist as condensed phases in the melt. Hence, their release is probably controlled by convective mass transfer from the melt. The oxygen content of the melt will be used to determine the dominant chemical form and volatility of these fission products. The behavior of the medium and low volatile fission products will be discussed in Section 5.3. The effect of a crust of U-Zr-O material surrounding the melt will be investigated in Section 5.4.

5.1 Geometry of the Molten Pool

For all fission product release calculations, the pool was assumed to be a hemisphere, 1.45 m in radius and 6385 L in volume. The details of pool growth during Phase 3b have been neglected. This volume represents 35% of the original core material. Based on metallurgical examination of samples that relocated from this region into the lower plenum, the material was found to be stoichiometric (U,Zr)O₂ with a melting point of ~2800 K. Potential fission product inventories in the pool are 35% of the total core inventories given in Table 1. Physical properties of the molten (U,Zr)O₂ used in these calculations are listed in Table 4.

TABLE 4. VALUES OF PHYSICAL CONSTANTS OF MOLTEN (U,Zr)O₂ AT 2800 K^a

Constant	Value	Range
Density, ρ (kg/m ³)	8700	--
Viscosity, μ (kg/m-s)	5.1 E-03	±25%
Heat capacity, c_p (J/kg-K)	500	±50%
Coefficient of thermal expansion, β (K ⁻¹)	9.3 E-05	+100%/-50%
Thermal conductivity, k (W/m-K)	4	±25%
Thermal diffusivity, α (m ² /s)	9.1 E-07	±50%
Kinematic viscosity, ν (m ² /s)	5.9 E-07	±25%

a. From References 13 and 33.

5.2 Volatile Fission Product Release from the Melt

The release of noble gases, Kr and Xe, and the volatile fission products, I and Cs is expected to be dominated by bubble dynamics in the molten pool because these high volatile fission products are gaseous at the high temperatures (>2800 K) in the melt. Results from the heatup analysis of this molten mass suggest that a large temperature gradient existed between the center and periphery of the melt and that the pool was probably in natural convection during Phase 3b.[28] As a result, gas bubbles in the melt can only be released if the buoyant velocity of the bubble is large enough to overcome the convective velocity in the pool. Comparison of the bubble rise velocity with the convective velocity in the pool will determine the critical bubble size that can escape from the pool and be released. This approach should provide a conservative estimate of the critical bubble size because it is assumed that the convective pool forces always oppose the buoyant forces of the bubble. However, given the circular nature of convection cells, it is recognized that sometimes the convective and buoyant forces act together to bring bubbles to the surface.

The rise velocity of a spherical gas bubble is found by balancing the drag and buoyant forces on the bubble. Hence

$$V_{\text{rise}} = 2\rho g r^2 / 9\mu \quad (8)$$

where

- ρ = density of melt (kg/m³)
- g = acceleration due to gravity (m/s²)
- r = radius of bubble (m)
- μ = viscosity of melt (kg/m-s).

The convective velocity can be obtained from an energy balance and is given by

$$V_{\text{conv}} = 2Q / \rho A c_p \Delta T \quad (9)$$

where

- Q = total decay energy in the pool (J)
- A = area for convection (m²)
- c_p = heat capacity (W/m-K)
- ΔT = temperature gradient from pool center to surface (pool superheat) (K).

The velocity given by Equation (9) more closely represents the velocity in the boundary layer than the velocity in the pool because most of the temperature gradient across the pool is in the boundary layer. The pool velocity is probably significantly larger than that given by Equation (9).

The criterion for bubble escape is given by

$$V_{rise} > V_{conv} \quad (10)$$

Solving for the critical diameter yields

$$d_{crit} > (18\mu V_{conv}/\rho g)^{1/2} \quad (11a)$$

$$d_{crit} > (90\mu/\rho^2 g A c_p \Delta T)^{1/2} \quad (11b)$$

Values for the variables used in Equations (8) through (11) are given in Tables 4 and 5. Realistic estimates of the ranges of these parameters are also listed in the table. Substituting the nominal values of the variables yields a minimum critical diameter of about 37 μm . The major uncertainty in this calculation is the pool convection velocity (V_{conv}), which in turn depends on the pool superheat (ΔT). Because most of the temperature gradient is in the boundary layer of the convecting pool, the nominal value of ΔT is probably too high. A lower temperature gradient through the pool would cause V_{conv} to increase. As a result, convection velocities between 0.1 and 10 cm/s were used to bracket the range of d_{crit} . Using these upper and lower estimates on the pool convection velocity results in a range for d_{crit} between 33 and 328 μm .

Having calculated the critical diameter of bubbles that will escape the pool, the amount of gas in the melt that is in bubbles greater than d_{crit} needs to be estimated. Most of the initial volatile fission product inventory will be in bubbles much less than d_{crit} . The initial bubble size in the pool is probably governed by the initial bubble distribution in the fuel grains prior to liquefaction. For the low burnup fuel in TMI-2, the gas bubbles in solid fuel are rather small ($\sim 100 \text{ \AA}$). However, as the fuel is dissolved and temperatures increase, diffusion of volatile fission product atoms in the fuel matrix and bulk diffusion of the intragranular gas bubbles in the fuel will cause most of the gas to reside in bubbles. These bubbles will interact and grow by coalescence. Coalescence theory can be used to determine the growth characteristics of the bubble size distribution in the molten pool and hence estimate how much gas release can be expected during Phase 3b.

The rate of coalescence of a bubble of radius r is given by [29]

$$dn_k/dt = 0.5 \sum_{i+j=k} B(r_i, r_j) n_i n_j - n_k \sum_{i=1}^{\infty} B(r_k, r_i) n_i \quad (12)$$

TABLE 5. VALUES OF PARAMETERS USED IN PHASE 3b RELEASE CALCULATION

Parameter	Value	Range
Pool internal heat generation, Q (MW/m ³)	1.75	±0.25
Pool superheat, ΔT(K)	198	128-320
Pool velocity, V _{conv} (cm/s)	0.13	0.1-10
Critical diameter, d _{crit} (μm)	37	33-328
Raleigh number, Ra	4.81 E+15	5.10 E+14/3.68 E+16
Prandtl number, Pr	0.65	--
Diffusion coefficient (cm ² /s)		
Ru	1.31 E-04	
Sr	4.24 E-05	
Sb	6.58 E-05	
Eu ₂ O ₃	3.27 E-05	
Ce ₂ O ₃	3.24 E-05	

where

$B(r_i, r_j)$ = coalescence frequency function (cm³/s)

n_k = number concentration of bubble of size r_k (p/cm³).

The first term represents the rate at which bubbles of size k are formed by collisions of particles of size i and j . The second term represents the rate at which bubbles of size k disappear due to coalescence with bubbles of all other sizes. Two processes are assumed to cause bubble coalescence: turbulence in the molten pool and differential bubble rise due to buoyancy. For each mechanism, a coalescence frequency function can be determined. Although not exactly applicable to the case of turbulence in the pool, a correlation for aerosol agglomeration in turbulent pipe flow is used.[30] It is given by

$$B(i, j)_{\text{turb}} = 1.3(r_i + r_j)^3 (\epsilon_d/\nu)^{1/2} \quad (13)$$

where

$$\epsilon_d/\nu = (4/d_m)(f/2)^{1.5} v_{\text{conv}}^3 \quad (14)$$

and

ϵ_d = eddy diffusivity (m²/s³)

ν = kinematic viscosity (m²/s)

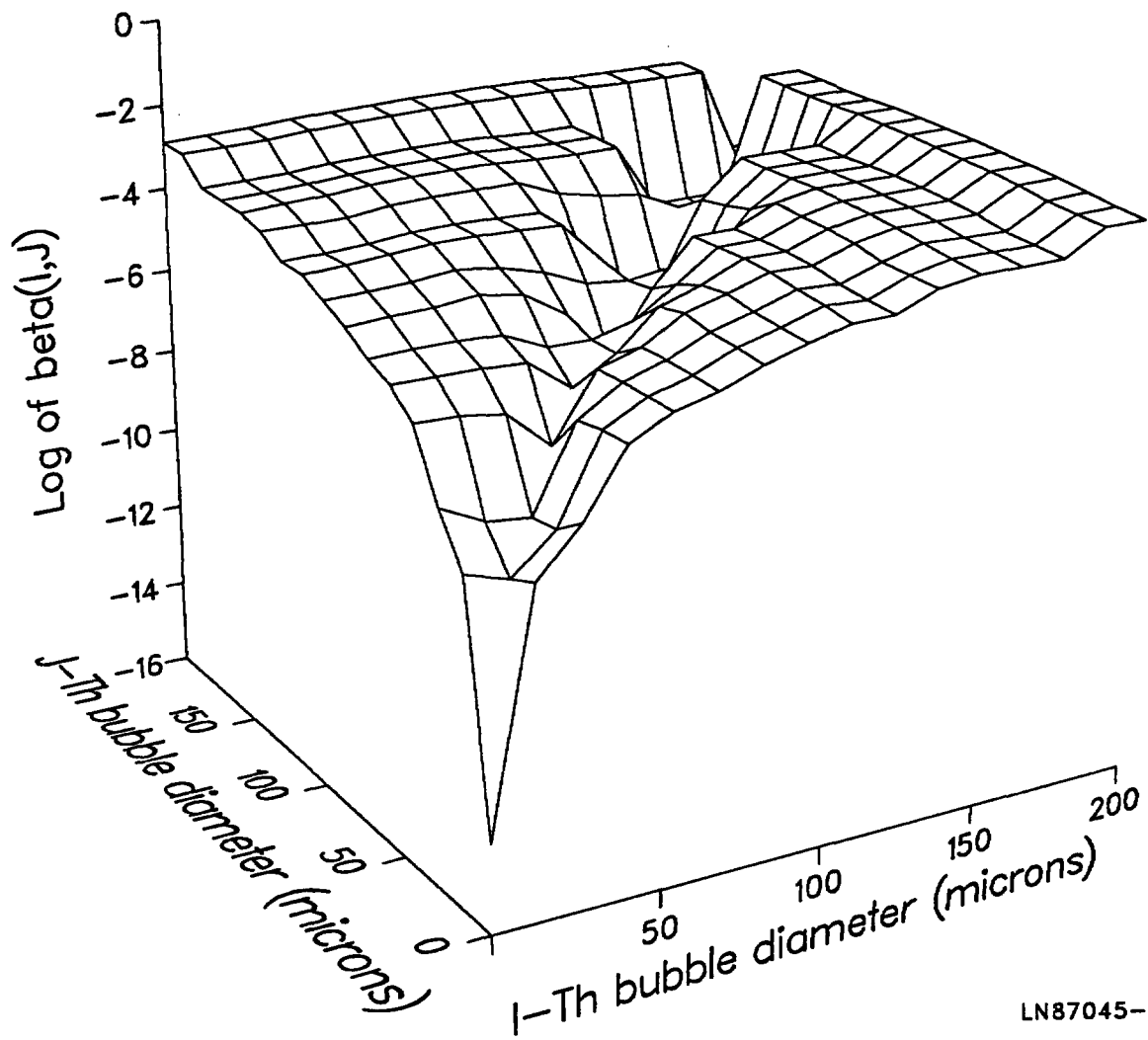
d_m = pool diameter (m)
 f = fanning friction factor (= 0.004)
 V_{conv} = pool convection velocity (m/s).

The rate of coalescence due to turbulence is found to be more sensitive to the velocity of the convecting pool than to the size of the bubble. For differential bubble rise in the pool, the frequency function is given by [30]

$$B(i,j)_{rise} = \pi(r_1 + r_j)^2 |V_1 - V_j| \quad (15)$$

As can be seen by examination of Equation (15), two bubbles of the same size will never coalesce through bubble rise since they rise at the same rate. For the analysis here, it is assumed that the overall collision frequency function is given simply as the sum of the turbulent and bubble rise functions. Figure 11 is a three-dimensional plot of the overall collision frequency function $B(i,j)$ as a function of the diameters of the two coalescing bubbles. As indicated in the plot, the frequency function increases dramatically as the size of either of the two coalescing bubbles increases. This result basically reflects the fact that large bubbles can sweep out more of the gas in the pool than small bubbles due both to their greater surface area and larger rise velocities. An examination of Equation (15) indicates that a factor of 10 increase in bubble radius will cause a factor of 10^4 increase in the coalescence frequency function. Separate examinations of the turbulent and bubble rise mechanisms indicate that turbulence is only important for very small bubbles. At large sizes, coalescence is due primarily to bubble rise in the pool. In Equations (12) through (15) it is assumed that each collision results in coalescence. This is a common assumption used in both UO_2 fuel swelling analysis and aerosol agglomeration theory.[29,30] Despite this fact, it is not clear that this assumption is correct for very small bubbles. The effects of bubble surface tension may result in only a fraction of all collisions producing coalescence. Nevertheless, the assumption that all collisions produce coalescence is used for this scoping type of study.

Due to the large uncertainty in many of the input parameters in this model, several calculations have been performed to bound the amount of gas that is released from the melt as a function of time. Three parameters were thought to control gas release from the pool. They are: (a) the amount of gas initially in the melt, (b) the initial size of the bubbles in the pool, and (c) the velocity in the pool (which determines the critical bubble diameter for escape and the rate of coalescence due to turbulence). Analysis of diffusional release during Phase 2 indicates that between 0 and 60% of the volatile fission products would have been released from individual fuel pellets (depending on their location in the core) prior to the formation of the molten mass. The fuel fracturing that occurred during the pump transient could have increased these values to close to 100% for some of the small fuel fragments. Because of this range in release estimates, no single initial inventory of gas in the melt can be estimated with certainty. As a result,



LN87045-1

Figure 11. Coalescence frequency function, $B_{i,j}$, as a function of bubble diameter.

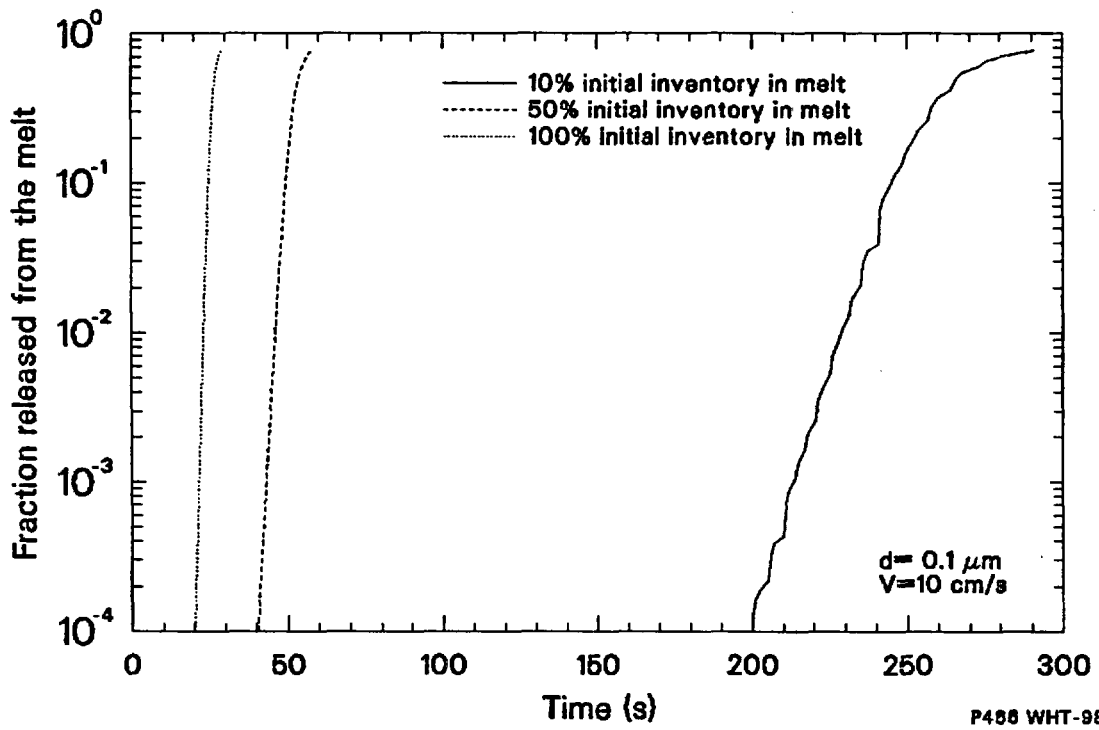
the sensitivity calculations were performed assuming that the pool contains 100%, 50%, and 10% of its initial inventory. Three initial bubble sizes of 0.01, 0.1, and 1 μm were chosen for the analysis. Finally, as stated earlier, due to uncertainties in pool thermal parameters, natural convection pool velocities ranging from 0.1 to 10 cm/s were chosen for this analysis.

The amount of gas release as a function of time for the best estimate case is shown in Figure 12. As indicated in the figure, release is very small early in time as the initial bubble distribution coalesces into larger bubbles. Once a sufficient quantity of large bubbles have developed, the amount of gas escaping the melt increases dramatically due to the sweeping effect of these bubbles. The results from this best estimate case indicate that most of the gas would be released from the melt during Phase 3b very quickly (<5 min). The times to release 75% of the volatile gas inventory from the melt for all the sensitivity cases are listed in Table 6. The results of all of the calculations indicate that virtually all of the gas would be released from the melt during Phase 3b. These results agree with the iodine retention estimates from the lower plenum samples, yet are in disagreement with the Cs retention data. Thus, it is postulated that the high cesium retention in the lower plenum samples is not the result of a physical process, but may be because the retained cesium is in a less volatile (as yet unknown) chemical form which reduces its volatility in the melt. Silicates, zirconates, and borates of cesium are three potential low volatile chemical forms that might be stable at 2800 K. Silicates could be formed from SiO_2 impurities in the stainless steel, borates could be formed by the interaction of B_4C burnable poison rods with the cesium, and zirconates could form by reaction of the cladding with cesium.

TABLE 6. VOLATILE FISSION PRODUCT RELEASE RESULTS FOR VARIOUS BUBBLE COALESCENCE PARAMETER VALUES

d_0 (μm)	V_{COBY} (cm/s)	Fraction of Initial Inventory (%)	Time to Release 75% of Inventory (s)
0.1	0.1	100	109
0.1	1.0	100	67
0.1	10.	100	29
0.01	10	100	66
0.1	10	100	29
1.0	10	100	8
0.1	10	100	29
0.1	10	50	57
0.1	10	10	291
0.1	10	100	369 ^a

a. Coalescence rate determined from turbulence alone. Bubble rise was not considered.



P486 WHT-987-01

Figure 12. Volatile gas release from the melt due to bubble coalescence and rise.

5.3 Medium and Low Volatile Fission Product Release from the Melt

Unlike the volatile fission products, the medium and low volatile fission products will tend to remain as condensed phases in the melt because of their low vapor pressures. The chemical forms of the lower volatile fission products in the melt are determined by the oxygen potential in the melt. As indicated in Figure 13, the high oxygen potential of stoichiometric $(U,Zr)O_2$ at 2800 K (-590 kJ/mole O_2) suggests that Eu and Ce will exist as oxides (i.e., Eu_2O_3 , and Ce_2O_3) whereas Ru, Sr, and Sb will exist as metals because of their low oxidation potentials.

Release of these materials from the molten pool can be calculated based on mass transport through a liquid. The rate of mass transport of a species in a liquid is given by

$$M_{vap} = k_c A (C_{bulk} - C_{surface}) \quad (16)$$

where

k_c = mass transport coefficient through the condensed phase (m/s)

A = surface area for vaporization (m^2)

C_{bulk} = bulk concentration of species in the melt (kgmole/ m^3)

$C_{surface}$ = concentration of species at the surface (kgmole/ m^3).

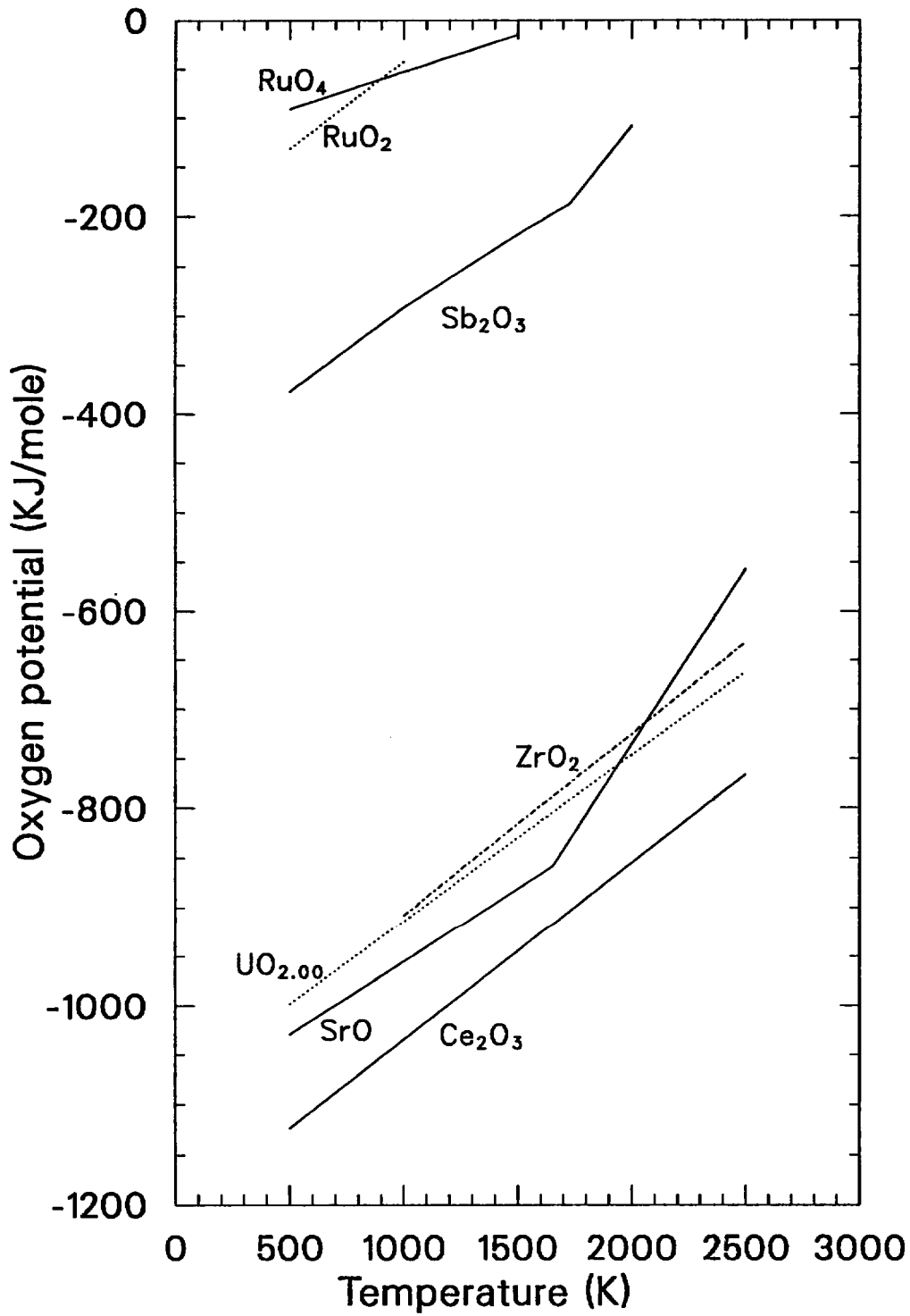
Assuming that the concentration at the surface is much smaller than the bulk concentration, a mass balance on the pool yields

$$dC/dt - M_{vap}/V = -(k_c A/V) * C \quad (17)$$

where V is the volume of the pool. The solution to Equation (17) is a simple exponential with a time constant of $(V/k_c A)$. The time constant is a function of the geometry and mass transport coefficient. The mass transport coefficient is determined by the hydrodynamics of the pool. Three extreme cases have been examined: (a) a stagnant pool where mass transport is controlled by diffusion, (b) a well-mixed pool where mass transport is controlled by natural convection of vapor to the pool surface, and (c) mass transport of vapor to the volatile fission gas bubbles in the pool.

For the pure diffusion calculation, the pool was modeled as a parallelepiped with a volume and height equal to that of the hemispherical pool ($V = 6385$ L, $R = 1.45$ m). For this geometry, the mass transport coefficient is given by [31]

$$k = (3 + \pi)\pi D / [R(1 + 4\sqrt{2\pi/3})] \quad (18)$$



P466-WHT-987-07

Figure 13. Free energies of formation for core material oxides.

where

D = diffusion coefficient of condensed phase in the melt (m^2/s)

R = radius of pool (m).

For the case where transport in the pool is controlled by natural convection, the mass transport coefficients for the top and bottom of the pool can be obtained from heat transfer correlations and the mass transfer analogy.[32]
Thus

$$Nu_{top} = 0.36 Ra^{0.23} (Sc/Pr)^{0.23} \quad (19)$$

$$Nu_{bottom} = 0.6 Ra^{0.2} (Sc/Pr)^{0.2} \quad (20)$$

where

Ra = Rayleigh number of the pool

Sc = Schmidt number

Pr = Prandtl number.

The Rayleigh, Schmidt, and Prandtl numbers are given by

$$Ra = (gBQR^4/\alpha\nu k), \quad Sc = \nu/D \quad \text{and} \quad Pr = \nu/\alpha \quad (21)$$

where

B = thermal expansion coefficient (K^{-1})

Q = volumetric heat generation in the pool (W/m^3)

α = thermal diffusivity (m^2/s)

k = thermal conductivity ($W/m-K$).

The average mass transport coefficient for the pool is given by surface area averaging Nu_{top} and Nu_{bottom}

$$k_c = (D/R)(Nu_{top} + 2Nu_{bottom})/3 \quad (22)$$

The diffusion coefficient for a condensed phase in the melt is given by [33]

$$D = 8.2 E-10 [1 + (3v_b/v_a)^{2/3}] T/(\mu_b v_a^{1/3}) \quad (23)$$

where

- D = diffusion coefficient (cm²/s)
μ_b = viscosity of the melt (g/cm-s)
v_a = molar volume of the melt (cm³/gmole)
v_b = molar volume of the condensed phase (cm³/gmole)
T = temperature of melt (K).

For the case of mass transport to the volatile gas bubbles, a transport time can be estimated using the equation for diffusion to a sphere [31]

$$\tau = R^2/(\pi^2 D) \quad (24)$$

where the characteristic size, R, is the radius of the bubble. Values of the parameters used to calculate the mass transport results are listed in Table 5.

Time constants have been calculated for the various fission product species using Equations (17) through (24). The results are presented in Table 7. The time constants associated with pure diffusion to the pool surface are extremely long for all species due to the small surface to volume ratio of the molten pool. As expected, the time constants for the well-mixed pool are smaller than those for diffusion. By contrast, the time constant associated with diffusion to a 10-μm bubble for all species is well under one second. This rapid transport time does not indicate however, that large release of the medium and low volatile fission products would be expected. The vapor concentration, C_{bulk}, of these fission product species in the melt needs to be examined. Raoult's law can be used to estimate the vapor concentration of the fission product oxides (Eu₂O₃, Ce₂O₃) because they are soluble in the ceramic melt. The low vapor pressures of Eu₂O₃ and Ce₂O₃, combined with their low mole fractions in the melt, result in a very small vapor concentration. Although the metallic fission products (Ru and Sb) have moderate vapor pressures at 2800 K, their vapor concentrations in the pool are also very small because of alloying of these species with other metallic components (Fe, Ni, Cr) [34,35] and the low mole fraction of metallic material in the molten pool. All of these thermodynamic arguments indicate that despite the potential for very quick diffusional transport times to the volatile gas bubbles, very little release of these medium and low volatile fission products would be expected because of their low upper pressures and mole fractions in the molten pool during the accident. However, if the material that did not relocate to the lower plenum remained hot for many hours, then the results in Table 7 indicate that some release might have occurred very late in the accident. All of these results agree with the lower volatile fission product retention data in Table 2. For the fission product oxides (Eu₂O₃, Ce₂O₃), very little release was noted. The low retention of the metallic fission products (Ru and Sb) in the lower plenum ceramic samples is not the result of vaporization. Rather, the low

TABLE 7. TIME CONSTANTS FOR DIFFUSIONAL FISSION PRODUCT RELEASE FROM THE MOLTEN POOL

Species	Diffusion Without Convection ^a (days)	Natural Convection (h)	Diffusion to a 10 μ m bubble (s)
Ru	96	3.9	7.70 E-04
Sr	297	9.4	2.38 E-04
Sb	197	8.8	1.53 E-03
Eu ₂ O ₃	386	11.5	3.13 E-03
Ce ₂ O ₃	389	11.6	3.12 E-03

a. For a rectangular parallelepiped of the same volume as the pool and a height corresponding to the pool radius of 1.45 m.

retention in these ceramic samples reflects the fact that Ru and Sb are tied up with the other metallic components (Fe, Ni, and Cr) in the melt that were not sampled.

5.4 Effect of a Surrounding Crust

It is not expected that the crust would have any open cracks in it due to its self-sealing nature. Because the material at the crust/pool interface is at the melting point, any crack in the crust would tend to be plugged by the molten material and refreeze thus preventing release of volatile fission products until the large relocation of material at 224 min.

6. FISSION PRODUCT RELEASE DURING PHASE 4

Very little fission product release is expected during the core relocation in Phase 4 because it occurred so rapidly. Release during this phase is probably governed by the break-up dynamics of the molten column as it entered the water in the lower plenum. The extent of release will be a function of the amount of melt surface area and trapped fission products exposed to water during and following the relocation. Estimating fission product release under such conditions is very difficult because of the difficulty in characterizing the cracking and breakup of the molten material as it entered the lower plenum. Posttest examination of the fuel bundle in Test SFD 1-1 [21] indicated that significant cracking of the molten U-Zr-O mass contributed to the large fission gas release upon cooldown. Thus, the potential existed for significant release of volatile gas inventory during Phase 4, depending on the extent of fragmentation as the debris entered the lower plenum. However, based on the results from the Phase 3b coalescence calculations, very little gas is expected to be trapped in the molten material at the time of relocation.

7. SUMMARY AND CONCLUSIONS

Based on this preliminary analysis of fission product behavior during the TMI-2 accident, the following conclusions can be drawn concerning high, medium, and low volatile fission product release:

Volatiles (Noble gas, I, Cs, Te):

Volatile fission product release during Phase 2 was dominated by diffusion up to the point that significant liquefaction of the fuel occurred. Based on a series of sensitivity calculations, the average core-wide fission product release during this phase was within the range of 0 to 27%, though individual locations within the core may have experienced up to 60% release. The macrocracks and fuel intergranular fracturing observed in the fuel in the upper debris bed suggest that considerable additional release of fission gases and volatile fission products could have taken place upon reflood following the B-loop pump transient. These volatile fission product release results are generally consistent with the iodine and cesium retention data obtained from the upper debris samples.

Although in general Te release from the fuel pellets would be roughly similar to the Xe diffusional results, separate effects test data indicate that Te tends to become bound to unoxidized Zr in the cladding. As the Zr oxidizes, the Te is released and transported from the cladding. Therefore, it is expected that those areas of the TMI-2 core that experienced a high degree of oxidation should have high Te releases while more Te retention is expected in areas of low oxidation.

Bubble coalescence calculations indicate that following liquefaction and consolidation of the molten material into a large pool, volatile fission products should be released very quickly from the melt due to sweeping of small gas bubbles by large ones to the melt surface. However, the gas would probably be trapped inside the crust until it failed at 224 min. The molten fuel breakup and macrocracking that occurred during Phase 4 can result in release of any trapped volatile gas bubbles. The magnitude of the potential release depends on the extent of debris breakup as the molten material entered the lower plenum. These results are in agreement with the iodine retention data for the lower plenum samples. However, these results also indicate that the high cesium retention in the lower plenum samples is not the result of physical bubble trapping in the molten pool. It is postulated that the cesium is in a less volatile (as yet unknown) chemical form which reduces its volatility in the melt. Silicates, zirconates, and borates of cesium are three potential low volatile chemical forms that might be stable at 2800 K.

Medium (Ru, Sb) and Low (Eu, Ce) Volatile Fission Product Release:

The chemical forms of the medium and low volatile fission products are determined by the oxygen potential of the system. The oxygen potential of the molten (U,Zr)O₂ pool in TMI-2 suggests that Eu and Ce will exist as oxides (i.e., Eu₂O₃ and Ce₂O₃) while Ru, Sr, and Sb

will exist as metals. Very little medium and low volatile fission product release was calculated to have occurred during the TMI-2 accident primarily because of the low volatility of these species in both the solid and molten fuel and the low surface-to-volume ratio of the melt. These calculational results agree with the lower volatile (Eu, Ce) fission product retention data. The low retention of the metallic fission products (Ru and Sb) in the lower plenum ceramic samples is not the result of vaporization. Rather, the low retention in these ceramic samples reflects the fact that Ru and Sb are tied up with the other metallic components (Fe, Ni, and Cr) in the melt that were not sampled.

The fission product retention estimates developed in this study have been compared, to the extent possible, with retention data from lower and upper plenum samples. This analysis has been able to explain some of the measurement results, however additional work is still required to explain the high cesium retention in the lower plenum. The results from this study will be factored into the accident scenario to provide additional insight into the accident. In addition, the results of this study will be used to help resolve outstanding severe accident and source term issues relating to fission product release, transport, and chemical form.

8. REFERENCES

1. E. L. Tolman et al., TMI-2 Accident Evaluation Program, EGG-TMI-7048, February 1986.
2. E. L. Tolman et al., TMI-2 Accident Scenario Update, EGG-TMI-7489, December 1986.
3. B. G. Schnitzler and J. B. Briggs, TMI-2 Isotopic Inventory Calculations, EGG-PBS-6798, April 1985.
4. D. W. Akers et al., "Fission Product Behavior in the TMI-2 Core: Preliminary Evaluation of Transport and Chemistry," Proceedings of the Symposium on Chemical Phenomena Associated with Radioactivity Releases During Severe Nuclear Plant Accidents, Anaheim, CA, September 9-12, 1986.
5. R. H. Barnes et al., Xenon Diffusion in Single-Crystal and Sintered UO₂, BMI-1533, August 1961.
6. J. B. Melehan et al., Release of Fission Gases from UO₂ During and After Irradiation, BMI-1623, March 1963.
7. D. F. Toner and J. L. Scott, "Study of Factors Controlling the Release of Xenon-133 from Bulk UO₂," The 64th Annual Meeting of the American Society for Testing and Materials, Atlantic City, NJ, June 1961.

8. S. G. Prussin et al., "Release of Volatile Fission Products from UO₂," Proceedings of the American Nuclear Society Meeting on Fission Product Behavior and Source Term Research, Snowbird, UT, July 15-19, 1984.
9. A. H. Booth and G. T. Rymer, Determination of the Diffusion Constant of Fission Xenon in UO₂ Crystals and Sintered Compacts, CRDC-720, August 1958.
10. G. A. Berna et al., RELAP5/SCDAP/MOD0 Code Manual, Volume 1: Code Structure, System Models, and Solution Methods, Draft Preliminary Report, EGG-RTH-7051, September 1985.
11. G. T. Lawrence, "A Review of the Diffusion Coefficient of Fission-Product Rare Gases in Uranium Dioxide," Journal of Nuclear Materials, 71, pp. 195-218, 1978.
12. J. Belle, (ed.), Uranium Dioxide: Properties and Nuclear Applications, Naval Reactors, Division of Reactor Development, USAEC, 1961.
13. D. L. Hagrman and G. A. Reymann (eds.), MATPRO-Version 11, A Handbook of Materials Properties for Use in the Analysis of Light Water Reactor Fuel Rod Behavior, NUREG/CR-0497, TREE-1280, February 1979.
14. TMI-2 Accident Core Heat-up Analysis, A Supplement, NSAC-25, June 1981.
15. M. Silberberg et al., Reassessment of the Technical Bases for Estimating Source Terms, NUREG-0956, July 1986.
16. Analysis of Three Mile Island--Unit 2 Accident, NSAC-80-1, March 1980.
17. R. R. Hobbins, D. J. Osetek, and D. L. Hagrman, "In-Vessel Release of Radionuclides and Generation of Aerosols," Proceedings IAEA Symposium on Source Term Evaluation for Accident Conditions, Columbus, OH, October 28-November 1, 1985, International Atomic Energy Agency, 1986.
18. D. W. Akers et al., TMI-2 Core Debris Grab Samples--Examination and Analysis Part 1, GEND-INF-075, EG&G Idaho, Inc., September 1986.
19. W. Dienst, P. Hofmann, and D. K. Kerwin-Peck, "Chemical Interactions between UO₂ and Zircaloy-4 from 1000 to 2000°C," Nuclear Technology, 65, pp. 109-124, April 1984.
20. A. W. Cronenberg et al., "An Assessment of Liquefaction-Induced I, Cs and Te Release from Low and High Burnup Fuel," Proceedings of the International Meeting on Light Water Reactor Severe Accident Evaluation, Cambridge, MA, August 28-September 1, 1983.
21. Z. R. Martinson, D. A. Petti, and B. A. Cook, PBF Severe Fuel Damage Test 1-1 Test Results Report, NUREG/CR-4684, EGG-2463, October 1986.

22. A. D. Knipe, S. A. Ploger, and D. J. Osetek, PBF Severe Fuel Damage Scoping Test--Test Results Report, NUREG/CR-4683, EGG-2413, August 1986.
23. J. Rest and A. W. Cronenberg, "Modeling the Behavior of Xe, I, Cs, Te, Ba and Sr in Solid and Liquefied Fuel during Severe Accidents," Journal of Nuclear Materials (in press).
24. M. Osborne et al., "Experimental Studies of Fission Product Release from Commercial Light Water Reactor Fuel Under Accident Conditions," Nuclear Technology, 78, 2, August 1987, pp. 157-169.
25. G. D. McPherson, R. R. Hobbins, and P. North, "U.S. Department of Energy Severe Accident Technology and Analysis Program," International Conference on Nuclear Power Performance and Safety, Vienna, Austria, September 28-October 2, 1987, IAEA-CN-48/192.
26. A. W. Cronenberg and T. R. Yackle, "Intergranular Fracture of Unrestructured UO₂ Fuel During Film-Boiling Operation," Journal of Nuclear Materials, 84, pp. 295-318, 1979.
27. P. J. Fehrenbach et al., "High Temperature Transient Fission Gas Release from UO₂ Fuel: Microstructural Observations," Proceedings of the International ANS/ENS Topical Meeting on Thermal Reactor Safety, San Diego, California, February, 2-6, 1986.
28. M. Epstein and H. K. Fauske, The TMI-2 Core Relocation--Heat Transfer and Mechanism, FAI/87-49, July 1987.
29. D. R. Olander, Fundamental Aspects of Nuclear Reactor Fuel Elements, TID-26711, 1976.
30. S. K. Friedlander, Smoke, Dust and Haze: Fundamentals of Aerosol Behavior, New York: John Wiley & Sons, 1977.
31. H. S. Carslaw and J. C. Jeager, Conduction of Heat in Solids, Cambridge: Oxford University Press, 1959.
32. M. Jahn and H. H. Reineke, "Free Convection Heat Transfer with Internal Heat Sources, Calculations and Measurements," Proceedings of the 5th International Heat Transfer Conference, Tokyo, Japan, September 1974, Paper No. 28.
33. D. A. Powers et al., VANESA: A Mechanistic Model of Radionuclide Release and Aerosol Generation During Core Debris Interactions with Concrete, NUREG/CR-4308, SAND85-1370, July 1986.
34. R. K. McCardell et al., "TMI-2 Core Bore Examination Results," 15th Water Reactor Safety Meeting, Gaithersburg, MD, October 26-29, 1987.

35. G. W. Parker et al., "Source Term Evaluations From Recent Core Melt Experiments," Proceedings IAEA Symposium on Source Term Evaluation for Accident Conditions, Columbus, OH, October 28-November 1, 1985, International Atomic Energy Agency, 1986.